



# A Hybrid Optoelectronic Sensor Platform with an Integrated Solution-Processed Organic Photodiode

Alexander Scholz, Daniel Gerig, Lukas Zimmermann, Mervin Seiberlich, Noah Strobel, Gerardo Hernandez-Sosa, and Jasmin Aghassi-Hagmann\*

Hybrid systems, unifying printed electronics with silicon-based technology, can be seen as a driving force for future sensor development. Especially interesting are sensing elements based on printed devices in combination with silicon-based high-performance electronics for data acquisition and communication. In this work, a hybrid system integrating a solution-processed organic photodiode in a silicon-based system environment, which enables flexible device measurement and application-driven development, is presented. For performance evaluation of the integrated organic photodiode, the measurements are compared to a silicon-based counterpart. Therefore, the steady state response of the hybrid system is presented. Promising application scenarios are described, where a solution-processed organic photodiode is fully integrated in a silicon system.

## 1. Introduction

In the future, the internet of things (IoT) will massively grow and computing as well as sensing devices will merge with the

A. Scholz, Prof. J. Aghassi-Hagmann  
Institute of Nanotechnology  
Karlsruhe Institute of Technology  
Eggenstein-Leopoldshafen 76344, Germany  
E-mail: jasmin.aghassi@kit.edu

A. Scholz, D. Gerig, Prof. J. Aghassi-Hagmann  
Institute for Applied Research  
Offenburg University of Applied Sciences  
Offenburg 77652, Germany

L. Zimmermann  
Institute of Reliable Embedded Systems and Communication Electronics  
Offenburg University of Applied Sciences  
Offenburg 77652, Germany

M. Seiberlich, N. Strobel, Dr. G. Hernandez-Sosa  
Light Technology Institute  
Karlsruhe Institute of Technology  
Karlsruhe 76131, Germany

A. Scholz, Prof. J. Aghassi-Hagmann, M. Seiberlich, N. Strobel,  
Dr. G. Hernandez-Sosa  
InnovationLab  
Heidelberg 69115, Germany

 The ORCID identification number(s) for the author(s) of this article can be found under <https://doi.org/10.1002/admt.202000172>.

© 2020 The Authors. Published by WILEY-VCH Verlag GmbH & Co. KGaA, Weinheim. This is an open access article under the terms of the Creative Commons Attribution-NonCommercial License, which permits use, distribution and reproduction in any medium, provided the original work is properly cited and is not used for commercial purposes.

DOI: 10.1002/admt.202000172

environment and become pervasive in our everyday life.<sup>[1]</sup> In this context, emerging technologies bring novel materials that allow new device types and system architectures. One promising research field is additive manufacturing, particularly printed electronics (PE) that offers the capability of large-area, low-cost, on-demand fabrication, as well as flexible substrates and new form factors.<sup>[2–8]</sup> Current research trends go into the direction of large-area sensors, actuators, flexible electronic circuits that can possibly stretch over arbitrarily curved surfaces, to name but a few.<sup>[5,9,10]</sup> In general, the unique properties of PE can be utilized in a complementary manner to conventional silicon-based technology. Thereby, the most

beneficial properties of both technologies can be exploited and combined in the form of hybrid systems. This way, the high-performance capabilities of silicon-based electronics can be paired with the large-area fabrication on non-uniform surfaces provided by PE.<sup>[3,5]</sup> Promising candidates for hybrid system implementations are large-area sensing applications that use classical silicon-based interfaces for data acquisition and communication with the outside world. In that regard, solution-processed organic photodiodes (OPDs) as light sensing systems are of great interest in current research.<sup>[11–15]</sup> As an example for smart homes, printed large-area light sensors can be used to detect spatial light conditions in the living space. In this scenario, a more sophisticated silicon-based computational unit could evaluate the signals that come from the printed sensors and control the lightning over wireless communication channels. Such a system should be flexible in terms of its measurement capabilities to allow DC and AC applications. Furthermore, it would require the capability to be calibrated if measurement variations occur over time, due to degradation effects in the organic devices.<sup>[16,17]</sup>

In this work, we propose a hybrid system that incorporates an OPD embedded into a silicon-based real-time sensor prototyping platform. The modular system architecture includes additional peripheral circuitry that can be configured as needed and operated in a realistic application environment. The hybrid system also incorporates a microcontroller that enables real-time experimental testing and verification of the OPD.

The herein presented sensor platform offers the following contributions in the field of hybrid optoelectronic systems:

- 1) We implement a solution-processed OPD, which can also be printed, within a silicon-based real-time system prototyping

platform. Furthermore, the OPD is compared with an off-the-shelf silicon-based photodiode for evaluation of the proposed system parameters.

- 2) The deployment of OPDs within such a framework enables application-driven development, which resembles a crucial pillar in holistic system development. For the envisioned applications prospective, a photometer and a light barrier with an OPD as sensing element are realized and further discussed within the presented platform.

## 2. Results

The hybrid optoelectronic sensor platform utilizes an integrated organic photodiode (OPD) with an active area of  $1\text{mm}^2$ , for measurement and possible application development along with silicon-based (Si) building blocks, as shown in **Figure 1**.

### 2.1. Hybrid Optoelectronic Sensor Platform Architecture

The presented hybrid optoelectronic sensor platform architecture is shown in **Figure 1**. The system is composed of a microcontroller development board for data communication with a personal computer. An attachable, self-designed printed circuit board hosts the OPD integration and development environment, which is referred to as optoelectronic integration board (OIB).

The OIB hosts various building blocks for OPD measurement and deployment of system application testing. An optical transmission stage (OTS) for signal transmission via an optical

fiber for dynamic OPD stimulation is deployed. The OTS can be controlled by the microcontroller or externally via a function generator. The transmission diode (SFH757V) in the OTS has a peak wavelength of  $\lambda_{\text{OTS}} = 650\text{nm}$ . For large area illumination, a high-power light-emitting-diode (LED) of the type GH CSSPM1.24 120 SSL, with a wavelength of  $\lambda_{\text{GH}} = 660\text{nm}$  is utilized, which is operated by an external current source. These wavelengths are chosen, since at this point, the integrated OPD shows a high spectral responsivity.<sup>[18,19]</sup> Further building blocks for signal processing and acquisition consist of a transimpedance amplifier (TIA), a 12-bit analog-to-digital converter (ADC), as well as passive high-pass filters and voltage regulators for on-board voltage generation of 1.2 V and 3.3 V, respectively. More information about the setup, circuitry, and used components can be seen in Experimental Section and Supporting Information, respectively. The building blocks required for OPD evaluation and experimental application design and verification are utilized in a flexible manner. The system can be configured as benchmarking and measurement platform, or being used for application development. This allows to evaluate the OPD's performance parameters and assess its suitability for different application scenarios.

### 2.2. Electrical Characterization and OPD Signal Analysis

We have evaluated the frequency behavior of the OPD with given TIA setup, utilizing the measurement setup 1 configuration as shown in **Figure 2a**. Device stimulation is performed with the OTS. For performance evaluation of the OIB and to

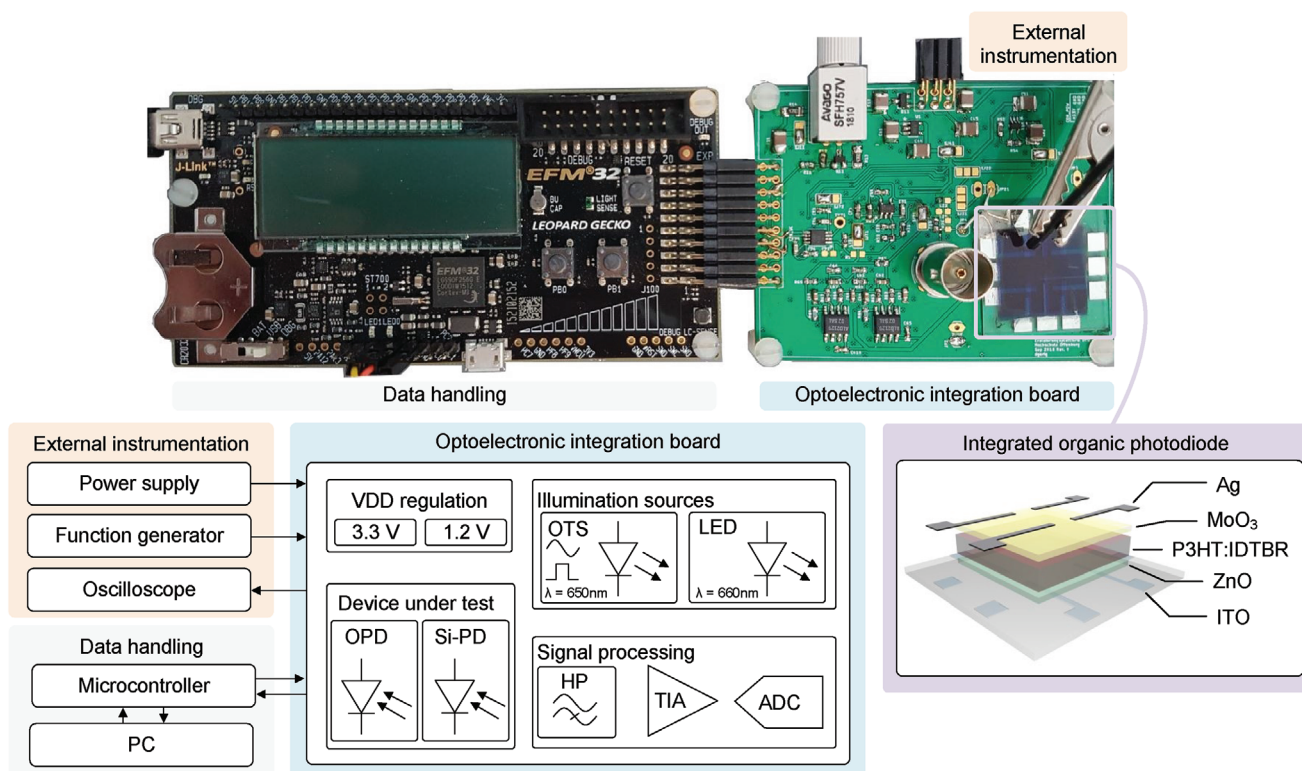


**Figure 1.** Hybrid optoelectronic sensor platform architecture and building blocks overview.

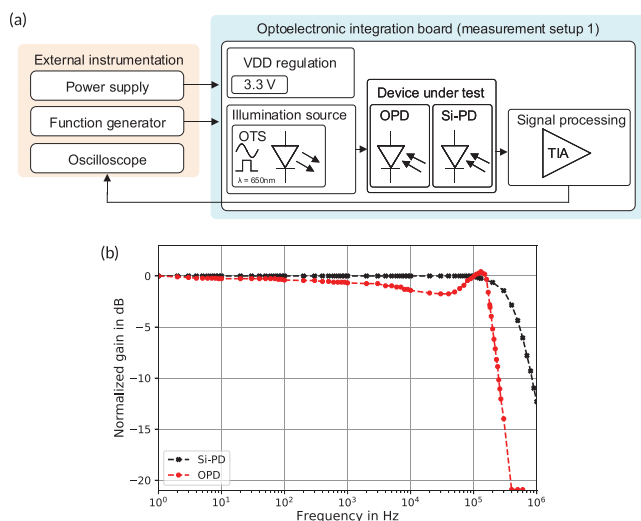


**Figure 2.** a) OIB setup (measurement setup 1) for PD frequency response measurements. b) Normed device frequency response of the Si-PD as reference (black line) and the OPD (red line) at an illumination wavelength of  $\lambda_{OTS} = 650$  nm and a reverse bias of 0.3 V.

provide a reference for OPD behavior, the OPD is compared to an off-the-shelf silicon-based photodiode (Si-PD) with an identical active sensitive area of  $1\text{mm}^2$ .

Figure 2b shows the normed device behavior of both photodiodes along the frequency range. The black line corresponds to the Si-PD, whereas the red line represents the behavior of the OPD. The Si-PD shows a flat response behavior along the frequency range, which serves as a performance benchmark for OPD operation and comparison. The possible operating frequency of the Si-PD exceeds the TIAs bandwidth by orders of several magnitudes. Therefore, the cutoff frequency of the TIA with the Si-PD connected at its input at 427 kHz is observed. The OPD shows a slightly damped frequency response behavior along the applied frequency range. Also, the TIA shows a gain peaking around  $\approx 182$  kHz with the OPD connected at its input. This is caused by the increased capacitance of the OPD in comparison with the Si-PD. The effect can be compensated by feedback capacitance adjustment of the TIA.<sup>[20]</sup> However, for evaluation and device comparison purposes, the same TIA setup is used and no further changes in compensation capacitance in the TIA feedback is deployed.

The steady state response of the hybrid system, with respect to varying illumination intensities, is evaluated with measurement setup 2, as shown in **Figure 3a**. Large area illumination is realized with an LED which is biased with a current-source-configured laboratory power supply. For measurements, the platform's ADC is used. By averaging 20 measured ADC samples, the resulting data points for the corresponding photocurrent ( $I_{photo}$ ) is extracted. The hybrid system allows a calibration of

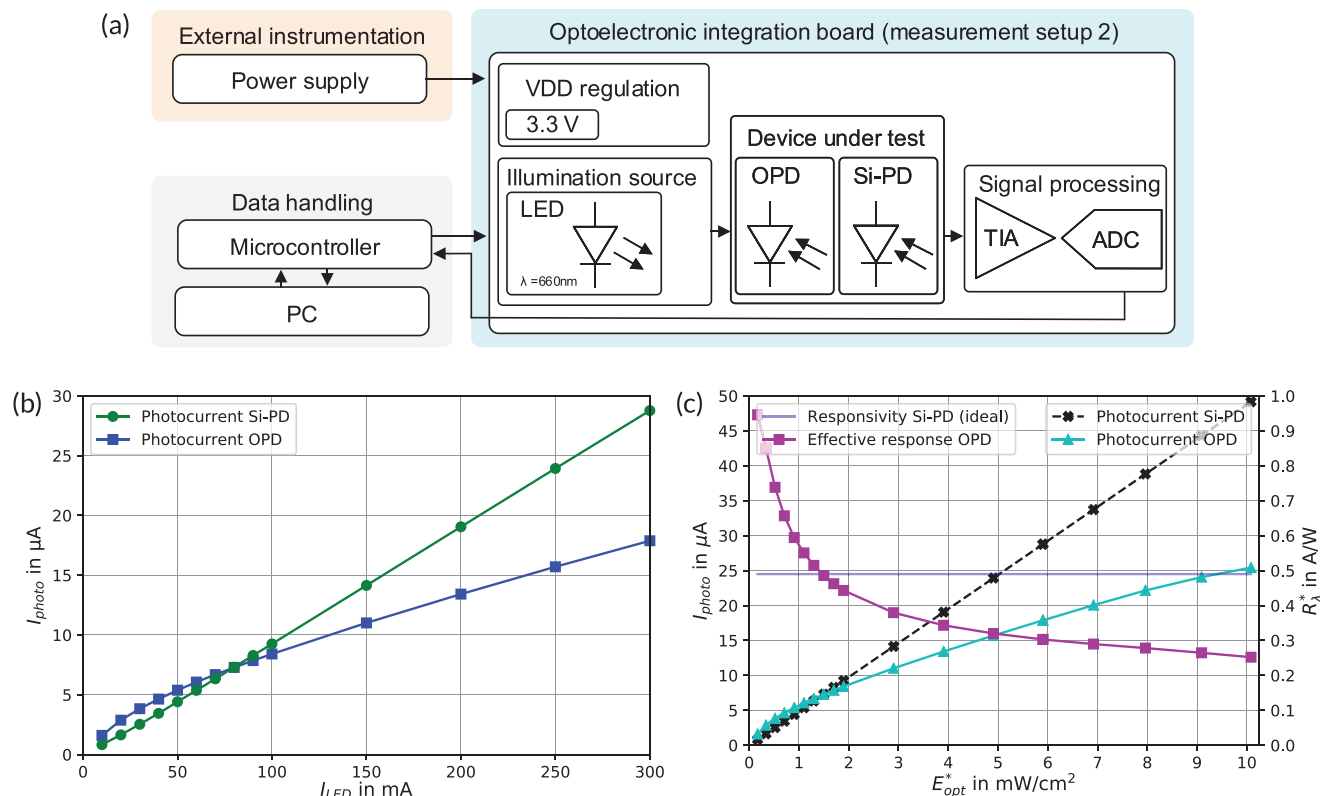


**Figure 3.** a) OIB setup (measurement setup 2) for effective response, photocurrent, dark current and noise measurements. b) Photocurrent over LED current at an illumination wavelength of  $\lambda_{CH} = 660$  nm and a reverse bias of 0.3 V. c) Photocurrent over corresponding calibrated irradiance for the Si-PD and OPD (black and light green lines) and reference responsivity of the Si-PD (blue line) as well as calculated effective response for the OPD (purple line) at an illumination wavelength of  $\lambda_{CH} = 660$  nm and a reverse bias of 0.3 V.

the measured photocurrent in an arbitrary environment. In our case, the calibrated irradiance  $E_{\text{opt}}^*$  of the light source is calculated from the measured photocurrent of the Si-PD. The corresponding Si-PD photocurrent per measurement point at a fixed LED diode current is divided by the active area and the Si-PD's responsivity  $R_\lambda$  at a wavelength of  $\lambda = 660 \text{ nm}$ , which is, for ease of evaluation, assumed linear over different irradiance levels ( $\approx 0.49 \text{ AW}^{-1}$ ) according to its datasheet.

Figure 3b shows both PD's photocurrents only over an applied LED current, which controls the LEDs irradiance. The Si-PD's photocurrent, over the calibrated irradiance, is illustrated in Figure 3c and shows a linear behavior. From this calibration, the effective response ( $R_\lambda^*$ ) of the hybrid system employing the OPD at the corresponding calibrated irradiance can be calculated. It should be noted, that this response cannot map the spectral responsivity of the OPD, as this would require a more advanced optical setup. Furthermore, for calibrated irradiance levels above  $5 \text{ mW cm}^{-2}$ , the TIA transimpedance is reduced to  $33 \text{ k}\Omega$  to further allow linear operation and avoid saturation of the TIA. In the presented measurement results, dark current effects are compensated. Therefore, the starting point for photocurrents at  $E_{\text{opt}}^* = 0 \text{ mW cm}^{-2}$  is at zero. The black and blue lines correspond to the Si-PD photocurrent and responsivity, accordingly, whereas the responsivity of the Si-PD is taken from the datasheet and plotted linearly as constant value, over  $E_{\text{opt}}^*$  for comparison purposes. The hybrid system employing the OPD shows a non-linear effective response. At illumination levels below  $1.5 \text{ mW cm}^{-2}$ , the OPD exceeds the Si-PD's responsivity, with values up to  $R_\lambda^* \approx 0.9 \text{ AW}^{-1}$ . However, with an increase in illumination strength, the photocurrent increases with a reduced steepness in comparison to the Si-PD. This leads to a lower effective response at higher intensity. We attribute this to a combination of effects stemming partly from the ambient illumination, light in-coupling through the glass substrate, intrinsic non-linearities of the simplified optical setup, as well as a temporal degradation of the OPD due to the delay of multiple weeks between the fabrication and implementation.<sup>[16,21]</sup> To understand the OPD material-specific degradation in detail, further studies are necessary in the future. For a complete and non-degraded overview of the OPD performance, we refer the reader to previous publications as refs. [13,18]. Nonetheless, the strength of the hybrid approach lies in the ability to compensate for different and non-standardized environments as well as for time-dependent changes (e.g., long term changes of the OPD output) through a calibration routine as shown in Section 2.3.1. For measurement of the OPD's dark and noise currents, the TIA feedback resistor is increased to

$10 \text{ M}\Omega$  for signal amplification. The Si-PD measurement results are used as a reference for the OPD measurements. For dark current measurements, 200 ADC samples in the dark state of the Si-PD and OPD are averaged to reduce the impact of noise. For noise current calculation, the standard deviation of the 200 sampled values are used. The calculated performance benchmark parameters are included in Table 1. For reference and performance comparison to the measured values, the Si-PD datasheet values are also given. This helps to predict systematic bias in the measurements, especially for noise measurements. The imbalance of noise current in the Si-PD datasheet value and its measured value is contributed due to environmental and the OIB system's noise floor. Furthermore, it should be noted that noise remains dependant over frequency. As the Si-PD is exposed over a broader frequency spectrum, direct value comparison of noise currents between both devices is difficult.

Nonetheless, the in-system measured OPD values are close to Si-PD values except the dark current, which is greatly increased. Therefore, dark current compensation strategies are required. This can be achieved with the adjustment of material properties.<sup>[22]</sup> The slight worse performance parameters in comparison to high-performance OPDs, which are presented in ref. [18], can be explained due to the effects of normalizing the irradiance according to the Si-PD values. Therefore, a minimal non-linear behavior, which exists also in Si-PD's, corresponds to the OPD measurements. Furthermore, the utilized OPD is utilized over months, where the device is showing slight degradation effects. Nonetheless, utilization of OPDs over longer time frames is a crucial point for system design evaluation, as strategies need to be developed to deal with degradation issues. However, for the given time frame, the used OPD shows still excellent device behavior and enables development in application scenarios within a system environment shown in the following section.

## 2.3. Application Scenarios for OPDs

### 2.3.1. Design and Implementation as Photometer

In the following, a photometer including another sample of the described OPD is investigated as possible application. In general, photometers can be utilized for transmission measurements in many applications. Therefore, the photometer needs to be capable to measure irradiance in a reliable manner. Based on our earlier works in the field of printed electronic circuits with electrolyte-gated transistors (EGTs), we propose a fully

**Table 1.** OPD parameter readout with OIB for in-system performance evaluation.

Parameter	Si-PD SH2400		OPD
	Datasheet value	Measured	Measured
Dark current <sup>a)</sup> (nA)	0.065	0.065	41.178
Noise current <sup>a)</sup> (pA)	9	53	113
Responsivity (Si-PD)   Effective response (OPD) <sup>b)</sup> ( $\text{AW}^{-1}$ )	0.49	—	0.95
Responsivity (Si-PD)   Effective response (OPD) <sup>c)</sup> ( $\text{AW}^{-1}$ )	0.49	—	0.25

<sup>a)</sup> $E_{\text{opt}}^* = 0 \text{ mW cm}^{-2}$ ; <sup>b)</sup> $E_{\text{opt}}^* = 169 \text{ }\mu\text{W cm}^{-2}$ ; <sup>c)</sup> $E_{\text{opt}}^* = 10.1 \text{ mW cm}^{-2}$ .

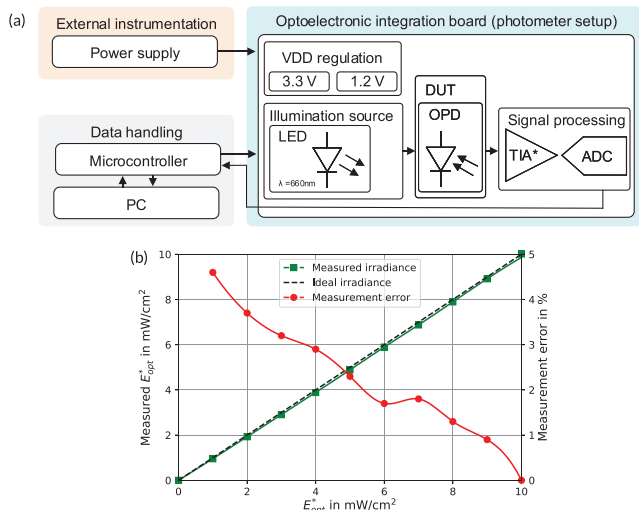


**Figure 4.** a) OIB setup for photometer application testing. The deployed TIA\* is based on a self-built analog transistor TIA. b) Linearized calibrated irradiance detection of the OPD over an applied calibrated reference irradiance.

printed OPD-TIA configuration for a photometer application. Therefore, we have used a DC-model of a n-type electrolyte-gated transistor<sup>[23]</sup> and simulated the current setup.

Printed TIAs based on EGTs could be deployed in the future. In **Figure 4a**, an exemplary setup for photometer deployment and evaluation is shown. The fabricated TIA is designed with an EGT SPICE model, while the hardware implementation is done with discrete analog n-type transistors that show similar electrical characteristics. The linearity achieved with the OPD and the emulated TIA system, is shown in **Figure 4b**. To evaluate the OPD linearity, a defined, calibrated irradiance  $E_{opt}^*$  at a wavelength of  $\lambda = 660\text{ nm}$  is applied to the OPD and the corresponding OPD irradiance is plotted. The LED is placed around 15 cm above the OPD.

The shown results are linearized using an interpolation strategy, as OPD photocurrent is not fully linear. This is done with a lookup-table, which is a common approach in embedded systems.<sup>[24]</sup> With this strategy, a good linearity with a relative error of  $<5\%$ , up to an applied calibrated irradiance of  $E_{opt}^* = 10\text{ mW cm}^{-2}$  is achieved, in comparison to perfect linear behavior. Furthermore, as irradiance levels increase, the relative error decreases and is at  $0.1\%$  at  $E_{opt}^* = 10\text{ mW cm}^{-2}$ . Therefore, the proposed and applied implementation strategy enables successful OPD deployment. The self-built TIA is further explained in the supporting information.

### 2.3.2. Design and Implementation as Light-Barrier

Another possible application for OPDs is a light barrier. Light barriers can be deployed to detect objects, which pass a defined light path. For the light barrier setup, the OIB is configured as shown in **Figure 5**, which can be categorized as fork light barrier. For OPD reverse biasing, a supply voltage of 3.3 V is used. Furthermore, the passive HP filters for DC-current suppression are deployed at the TIA input and output, respectively. The HP filter's cut-off frequency is at 3.5 kHz, for environmental

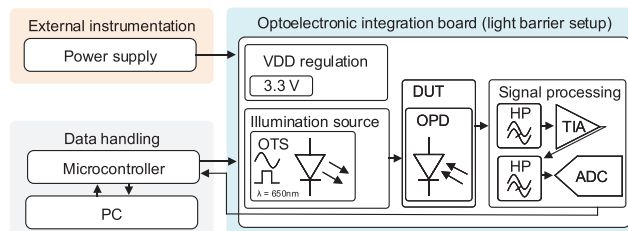


**Figure 5.** OIB setup for light-barrier application testing.

illumination, and general low-frequency noise suppression. A short signal pulse of  $3.3\text{ }\mu\text{s}$  within a  $333\text{ }\mu\text{s}$  signal period is applied to the OPD via the OTS. The OTS input is controlled via the microcontroller. This allows for a well-controlled synchronization between the sending impulse and the corresponding ADC readout. The OTS is set to its maximum operating power while transmitting the optical signal pulse to enable a high signal-to-noise ratio (SNR). The OTS fiber cable output is placed 2 cm close to the OPD. The proposed setup and implementation was shown in a real-time live demonstration.

## 3. Conclusions

With the given hybrid system approach, dynamic solution-processed OPD integration and application development are enabled. The herein presented approach helps to explore and tackle novel device capabilities as well as existing challenges, such as possible degradation in emerging OPDs. Implemented application examples derived with this setup include a photometer for transmission measurements and a light barrier for objective detection within a defined light path. The embedded OPD shows very good performance metrics within the system. The integrated OPD offers low noise currents of  $\approx 113\text{ pA}$ , an effective response of up to  $R_{\lambda}^* = 0.9\text{ AW}^{-1}$  at calibrated irradiance levels below  $1.5\text{ mW cm}^{-2}$ . However, the OPD's effective response does not remain stable over the measured calibrated irradiance and decreases with an increase in  $E_{opt}^*$ . Therefore, linearization strategies for OPD deployment as sensor are required, as demonstrated in the photodetector application. The OPD was passivated and utilized for testing over several months, which explains the slightly worse performance metrics than previously reported devices. However, stability in operation over time and general reliability of novel devices are important metrics for system development. The presented hybrid system utilizes PE-based and Si-based device benefits in a complementary manner. This means that the OPD could be fabricated on large-area flexible substrates for light-sensing applications, while the system backbone for communication and data transmission remains a silicon-based system, which might also be printed in the future. However, upscaling in numbers of novel devices, such as the utilized OPD and proper signal handling, are challenges to be tackled in the future.

## 4. Experimental Section

**OIB Building Blocks:** The OTS consisted of an emitter circuit (BC817), with the transmission diode (SFH757V) connected to its collector

output. A fiber cable was attached to the SFH757V package interface. Precise OPD stimulation could be performed via the fiber cable. An OPA377 operational amplifier, with a feedback resistance of 100 k $\Omega$  and a feedback capacitance of 4.7 pF for the TIA setup was used. The utilized linear regulators for on-board voltage levels were of the type ADP7142 for the required 3.3 V and TPS717 for the 1.2 V, respectively. Therefore, an external supply voltage of  $V_{bias} = 15V$  was fed to the input of the ADP7142. The regulated 3.3 V output voltage of the ADP7142 was further processed by the TPS717 to generate the 1.2 V. The corresponding voltage levels were realized by voltage dividers at the device outputs. The deployed 12-bit ADC was a MAX1237 with integrated inter-integrated-circuit (I<sup>2</sup>C) data bus for communication with the microcontroller. For all used OIB setups, the ADC reference voltage was at 3.3 V, except the photometer application, where a reference voltage of 1.2 V was utilized. With a reference voltage of 3.3 V, the ADC voltage resolution was therefore at 0.8 mV and with 1.2 V at 0.3 mV, respectively. As microcontroller, an EFM32 Leopard Gecko was used. The microcontroller  $\leftrightarrow$  personal computer communication was realized with a universal asynchronous receiver-transmitter (UART) interface. All microcontroller and ADC setup parameters could be controlled via a custom-built SciPy script.

**OIB Measurement Setup:** The Si-PD for performance comparison and  $E_{opt}$  deviation was of the type Osram SFH2400. For OPD frequency evaluation, a function generator (Keysight 33500B) was used to apply a sinusoidal signal to the OTS input. The output transmitting diode then applied a sinusoidal light signal to the device under test. By gradually increasing the light signal frequency, the frequency response of the photodiode was evaluated with an external oscilloscope of the type Keysight MSO-X3024T. In general, for the shown measurements, the photodiodes (Si-PD and OPD) were operated with a reverse bias of 0.3 V within the two measurement setups, as shown in Figures 2a and 3a, respectively. The transimpedance of the TIA was set up with a feedback resistor of 100 k $\Omega$ . This value was selected, to allow linear operation in a range of input currents up to 30  $\mu$ A. Furthermore, the TIA's cutoff frequency ( $f_c$ ) was at 427 kHz, with the Si-PD connected to its input, which sets the overall applicable system bandwidth as reference within the platform. However TIA bandwidth was dependent on the feedback resistance and input capacitance, and therefore also dependent on the connected photodiode's internal capacitance.

For measurements shown in Figure 3c, a GH CSSPM1.24 120 SS LED for large area illumination with a current source-configured power supply (HP E3631A) was utilized.

**OPD Fabrication:** OPD fabrication was carried out in a cleanroom environment under ambient conditions. The device architecture of the OPD array can be seen in Figure 1 (small inset). Pre-structured indium tin oxide (ITO) on glass was used as a transparent electrode and spin-coated 40 nm of zinc oxide (ZnO, Avantama N10) on top to form a hole blocking layer. A 200 nm thick spin-coated blend of P3HT (Rieke Metals, MW = 72 800) and IDTBR (I-Materials) served as the active layer in order to obtain a broadband OPD with a spectral range in the visible and near-infrared. For the ink, the active materials were dissolved in a 1:1 ratio with 40 g L<sup>-1</sup> in chlorobenzene. The architecture was finished with an evaporated 30 nm thick MoO<sub>3</sub> electron blocking layer and four evaporated 100 nm silver electrodes confining four pixels with the size of 1 mm<sup>2</sup>. The OPD was encapsulated with a glass slide and a UV-adhesive. More details regarding the fabrication and figure of merits of the OPD can be found in ref. [18]. To contact the OPD to the board, conducting silver paste was deposited on the silver electrodes and a small wire was attached, which was utilized for system integration.

## Supporting Information

Supporting Information is available from the Wiley Online Library or from the author.

## Acknowledgements

This work was supported by the Ministry of Science, Research, and Arts of the state of Baden Wuerttemberg, Germany through the Modellierung, Entwurf, Realisierung, und Automatisierung von gedruckter Elektronik und ihren Materialien (MERAGEM) doctoral program. D.G. thanks the Stiftung Industrieforschung for financial support. G.H.S acknowledges the financial support of the German Ministry for Education and Research (BMBF) under Grant No. FKZ: 03INT606AG. J.A.H. acknowledges the financial support of the German Ministry for Education and Research (BMBF) under Grant No. FKZ: 03INT606AF.

## Conflict of Interest

The authors declare no conflict of interest.

## Keywords

hybrid systems, inorganic/organic thin film devices, organic photodiodes, printed electronics

Received: February 28, 2020

Revised: April 16, 2020

Published online:

- [1] L. Atzori, A. Iera, G. Morabito, *Comput. Networks* **2010**, *54*, 2787.
- [2] K. Suganuma, *Introduction to printed electronics*, Vol. 74, Springer Science & Business Media, Berlin **2014**.
- [3] R. A. Street, T. N. Ng, D. E. Schwartz, G. L. Whiting, J. P. Lu, R. D. Bringans, J. Veres, *Proc. IEEE* **2015**, *103*, 607.
- [4] J. S. Chang, A. F. Facchetti, R. Reuss, *IEEE J. Emerg. Sel. Top. Circuits Syst.* **2017**, *7*, 7.
- [5] Y. Khan, A. Thielens, S. Muin, J. Ting, C. Baumbauer, A. C. Arias, *Adv. Mater.* **2019**, 1905279.
- [6] K. Fukuda, T. Someya, *Adv. Mater.* **2017**, *29*, 1602736.
- [7] G. Hernandez-Sosa, S. Tekoglu, S. Stolz, R. Eckstein, C. Teusch, J. Trapp, U. Lemmer, M. Hamburger, N. Mechau, *Adv. Mater.* **2014**, *26*, 3235.
- [8] Y. Khan, A. E. Ostfeld, C. M. Lochner, A. Pierre, A. C. Arias, *Adv. Mater.* **2016**, *28*, 4373.
- [9] H. Akkerman, B. Peeters, A. van Breemen, S. Shanmugam, D. Tordera, J.-L. van der Steen, A. J. Kronemeijer, P. Malinowski, F. D. Roose, D. Cheyins, J. Genoe, W. Dehaene, P. Heremans, G. Gelinck, in *SID Symp. Digest of Technical Papers*, Vol. 49, Wiley, New York **2018**, pp. 494–497.
- [10] J. Zimmermann, S. Schliske, M. Held, J.-N. Tisserant, L. Porcarelli, A. Sanchez-Sanchez, D. Mecerreyes, G. Hernandez-Sosa, *Adv. Mater. Technol.* **2019**, *4*, 1800641.
- [11] F. P. G. de Arquer, A. Armin, P. Meredith, E. H. Sargent, *Nat. Rev. Mater.* **2017**, *2*, 1.
- [12] M. Kielar, O. Dhez, G. Pecastaings, A. Curutchet, L. Hirsch, *Sci. Rep.* **2016**, *6*, 39201.
- [13] N. Strobel, M. Seiberlich, R. Eckstein, U. Lemmer, G. Hernandez-Sosa, *Flexible Printed Electron.* **2019**, *4*, 043001.
- [14] P. C. Y. Chow, T. Someya, *Adv. Mater.* **2019**, 1902045.
- [15] N. Strobel, N. Droseros, W. Köntges, M. Seiberlich, M. Pietsch, S. Schliske, F. Lindheimer, R. R. Schröder, U. Lemmer, M. Pfannmöller, N. Banerji, G. Hernandez-Sosa, *Adv. Mater.* **2020**, *32*, 1908258.
- [16] M. Kielar, M. Daanoun, O. François-Martin, B. Flament, O. Dhez, A. K. Pandey, S. Chambon, R. Clerc, L. Hirsch, *Adv. Electron. Mater.* **2018**, *4*, 1700526.

- [17] N. Gasparini, M. Salvador, S. Strohm, T. Heumueller, I. Levchuk, A. Wadsworth, J. H. Bannock, J. C. de Mello, H.-J. Egelhaaf, D. Baran, et al, *Adv. Energy Mater.* **2017**, 7, 1700770.
- [18] N. Strobel, M. Seiberlich, T. Rödlmeier, U. Lemmer, G. Hernandez-Sosa, *ACS Appl. Mater. Interfaces* **2018**, 10, 42733.
- [19] N. Gasparini, A. Gregori, M. Salvador, M. Biele, A. Wadsworth, S. Tedde, D. Baran, I. McCulloch, C. J. Brabec, *Adv. Mater. Technol.* **2018**, 3, 1800104.
- [20] KK Hamamatsu Photonics, *Opto-Semiconductor Handbook*, Hamamatsu Photonics KK, Solid State Division, Hamamatsu, Japan **2014**.
- [21] J. Euvrard, A. Revaux, A. Kahn, D. Vuillaume, *Org. Electron.* **2020**, 76, 105450.
- [22] G. Simone, M. J. Dyson, S. C. J. Meskers, R. A. J. Janssen, G. H. Gelinck, *Adv. Funct. Mater.* **2019**, 1904205.
- [23] G. C. Marques, S. K. Garlapati, D. Chatterjee, S. Dehm, S. Dasgupta, J. Aghassi, M. B. Tahoori, *IEEE Trans. Electron Devices* **2016**, 64, 279.
- [24] G. Van der Horn, J. Huijsing, *Integrated Smart Sensors: Design and Calibration*, Vol. 419, Springer Science & Business Media, Berlin **2012**.